## High Modulus Single-Ion-Conducting Electrolytes Based on a Rigid-Rod Polyanion

Joshua E. Bostwick, <sup>1†</sup> Deyang Yu, <sup>2†</sup> Curt J. Zanelotti, <sup>2</sup> Theo J. Dingemans, <sup>3</sup> Louis A. Madsen, <sup>2\*</sup> and Ralph H. Colby <sup>1\*</sup>

<sup>1</sup>Department of Materials Science and Engineering, Pennsylvania State University, University Park, Pennsylvania 16802, United States

<sup>2</sup>Department of Chemistry and Macromolecules Innovation Institute, Virginia Tech, Blacksburg, Virginia 24061, United States

<sup>3</sup>Department of Applied Physical Sciences, University of North Carolina, Chapel Hill, North Carolina 27599, United States

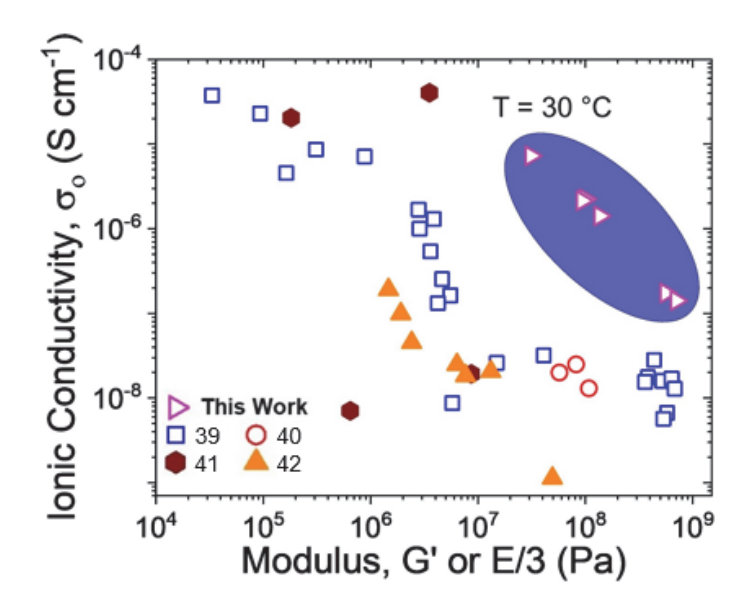
† Authors contributed equally

#### **Abstract**

Single-ion-conducting electrolytes enable easy processing and can block Li dendritic growth, showing potential for use in solid-state batteries. We report solid electrolytes that combine a rigid-rod polyanion, poly(2,2'-disulfonyl-4,4'-benzidine terephthalamide) (PBDT) with Na<sup>+</sup> or Li<sup>+</sup> counterions, and poly(ethylene glycol) (PEG,  $M_n = 400 \text{ g mol}^{-1}$ ). PBDT-PEG membranes show Young's modulus from 90 – 2110 MPa that increases with PBDT content and is > 4× higher for Li-based vs. Na-based electrolytes. We attribute this dramatically higher modulus in LiPBDT-PEG to poorer ion dissociation between Li<sup>+</sup> and PBDT sulfonate groups and stronger interactions between LiPBDT and PEG. These membranes show an increase in ionic conductivity with increasing PEG concentration (0.1 – 7  $\mu$ S cm<sup>-1</sup> at 30 °C), reaching 0.13 mS cm<sup>-1</sup> at 120 °C. These materials use highly rigid and charged PBDT double helices to "solidify" low molecular weight PEG into mechanically strong and highly single-ion-conductive solid polymer electrolytes with high thermal stability. Their combination of high cation conductivity and high modulus exceeds those of competing single-ion conductors at 30 °C.

**Keywords:** mechanical strength, ionic conductivity, ionic interactions, dielectric constant, solid electrolyte, thermal stability

# ToC Graphic:



#### Introduction

Lithium-ion batteries have widespread applications in portable devices, <sup>1, 2</sup> wearable electronics, <sup>3</sup> and hybrid/electric vehicles <sup>4</sup> due to their high energy density and long cycle life. These batteries generally rely on liquid electrolytes that are produced by dissolving a lithium salt in organic carbonate solvents such as propylene carbonate, ethylene carbonate, and diethyl carbonate. <sup>5</sup> This combination allows for high ionic conductivity (1 – 10 mS cm<sup>-1</sup>) which is needed for most commercial battery applications. <sup>6</sup> However, the solvents used in battery electrolytes are flammable and toxic, with a limited electrochemical stability and no resistance to lithium dendrite growth, which can cause internal short circuiting. <sup>7</sup> Additionally, when the solvents interact with a lithiummetal anode, the high chemical and electrochemical reactivity of the metal corrodes the anode, leading to low Coulombic efficiency and poor cyclability. Because of these issues, replacing liquid electrolytes with safer and more stable alternatives presents a continuing challenge.

Solid-state polymer electrolytes have potential for overcoming the shortcomings of liquid-based electrolytes. Since the discovery by Wright et al. of alkali-salt-poly(ethylene oxide) (PEO) electrolytes, polymer electrolytes have received intense investigation over the past several decades due to their high flexibility, low cost, and easy preparation. Some polymer electrolytes employ covalent bonding of the anion to the polymer to yield single-ion-conducting electrolytes that avoid both salt concentration polarization and dendrite growth during cell cycling. 11-13

While single-ion-conducting polymer electrolytes can minimize dendrite growth, their ionic conductivity is typically low due to the coupling effect between ionic conductivity and the glass transition temperature ( $T_g$ ) of the polymer matrix.<sup>6</sup> To increase ionic conductivity, plasticizers or solvents are usually added to the polymer electrolytes to form gel polymer

electrolytes (GPEs). GPEs combine the robust mechanical properties of the host polymer matrix with the fast ion transport dynamics of the solvents. <sup>14, 15</sup> By incorporating a high dielectric constant solvent, the mobile ions move with the enhanced motions of the gel matrix, thus enhancing ionic conductivity. <sup>16</sup> However, this plasticizing solvent leads to a mechanically weaker polymer network, reducing the potential for GPEs to serve as both the electrolyte and separator in a battery. Additionally, GPEs often suffer from instabilities, such as solvent evaporation under GPE preparation <sup>17</sup> and GPE melting at elevated (but still relatively low) temperature. <sup>18</sup>

To circumvent this tradeoff between the ionic conductivity and mechanical strength of GPEs, one promising method is implementing rigid polymers as the polymer matrix. <sup>19,20</sup> Poly(2,2'disulfonyl-4,4'-benzidine terephthalamide), or PBDT, is a rigid-rod sulfonated polyanion with alkali metal counterions. PBDT exhibits a double-helical conformation with an extremely high persistence length when dissolved in water,<sup>21</sup> as well as a nematic phase above a PBDT concentration ~ 1 wt%. 22 Recent electrolyte studies employing PBDT as a host matrix have incorporated ionic liquids (ILs), due to their high ionic conductivity and electrochemical stability, to form solid polymer electrolytes called molecular ionic composites (MICs).<sup>23-30</sup> These MIC electrolytes feature low PBDT concentration (4 - 25 wt%) and demonstrate a biphasic internal structure – a PBDT-rich bundle phase and a percolated IL-rich fluid phase.<sup>23, 25, 30</sup> The IL cations and anions form alternating layers around the PBDT double helix leading to a collective electrostatic network.<sup>31</sup> Because of this, MICs produce high ionic conductivities due to the highly mobile IL ions, and up to GPa tensile moduli<sup>23, 24</sup> and MPa shear moduli<sup>25</sup> due to the thermomechanical stability of the PBDT-rich bundle phase. Furthermore, Li-metal batteries using MICs as solid electrolytes can operate stably within a wide temperature range from room temperature to

150 °C.<sup>26</sup> Although MICs show promise for implementation as battery electrolytes, their high ionic conductivity mainly derives from the IL, leading to relatively low Li<sup>+</sup> transference number.

In this study, we present PBDT-based single-ion-conducting solid polymer electrolytes, with Na<sup>+</sup> or Li<sup>+</sup> counterions, fabricated by replacing the IL with low molecular weight polyethylene glycol (PEG). These materials exhibit exceptional mechanical properties and thermal stability as well as enhanced conductivity relative to other solid polymer single-ion conductors, thus opening a new avenue for safe and easily processable solid Li<sup>+</sup> conductors. By characterizing mechanical and dielectric responses as functions of PBDT concentration and mobile counterion type, we present understanding of how different PBDT-PEG compositions can give rise to desired properties needed for next-generation battery electrolytes.

# **Morphology and Mechanical Properties of PBDT-PEG Electrolytes**

By incorporating PEG into the PBDT matrix (structures shown in **Figure 1a**), free-standing electrolyte membranes with varying NaPBDT or LiPBDT concentration are obtained (**Figure 1b**). To understand their resulting morphology, we use atomic force microscopy (AFM) in tapping mode to obtain height and phase maps of the membranes. Previous studies have found that PBDT-based MIC electrolytes show a biphasic internal structure where one phase is dominated by a PBDT-rich "bundle" phase and the other is a percolated IL-rich "puddle" or fluid phase.<sup>23, 25</sup> The "bundle" phase provides cohesion via massively parallel PBDT-ion associations (albeit with fast ion transport due to individually weak associations), while the percolated fluid phase has little PBDT and thus behaves with liquid-like properties. **Figure 1c** demonstrates that the PBDT-PEG membranes show height and phase maps similar to the MIC electrolytes.<sup>28</sup> The fibril structures have higher phase angle and height, corresponding to the hard regions of the samples, while the

dark regions with lower phase angle and height relate to the soft domains of the samples. At low PBDT concentrations, the soft domains cover a large volume fraction of the membrane surface. Increasing the PBDT concentration leads to an increased volume fraction of the fibril phase, indicating that the fibers contain more PBDT polymer while the soft domains contain more PEG.

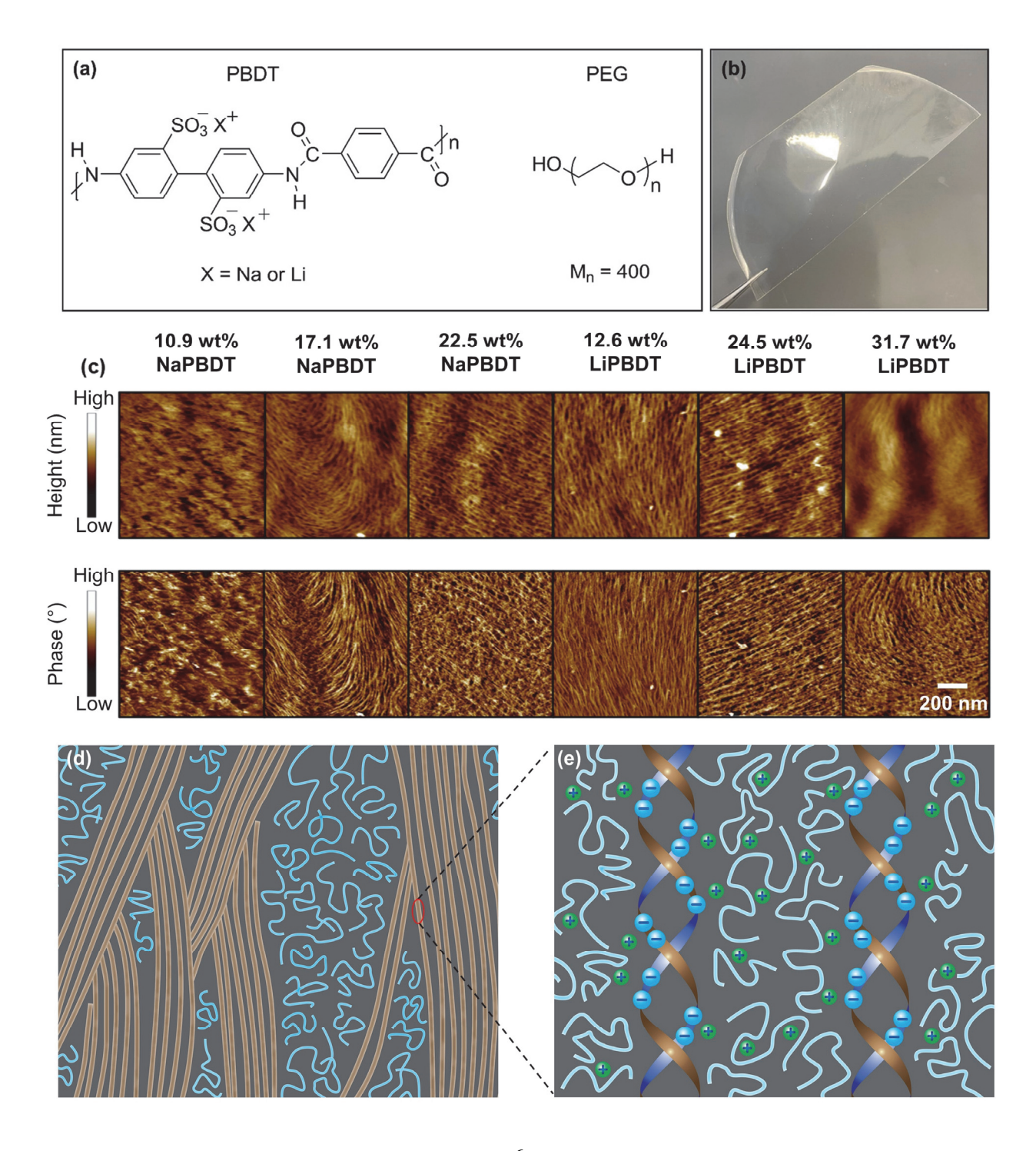


Figure 1: Morphology of PBDT-PEG Membranes. (a) Molecular structures of PBDT with Na $^+$  or Li $^+$  counterions and PEG400. (b) Image of a single-ion-conducting solid polymer electrolyte film containing 24.5 wt% LiPBDT with a thickness of 80  $\pm$  10  $\mu$ m. (c) Atomic force microscopy (AFM) tapping mode images of the PBDT-PEG membranes over a 1  $\mu$ m $^2$  area. Increasing the PBDT concentration in the membranes leads to the formation of a single-bundle phase. (d) Conceptual  $\sim$  100 nm scale model of the biphasic internal network of PBDT-PEG membranes (Li $^+$  or Na $^+$  form) where PBDT-rich bundles (orange lines) interact with PEG (blue lines). (e) Conceptual nanometer-scale model of the ionic interactions within a PBDT bundle. At a rod-rod distance of  $\sim$  2 nm, the counterions interact with both the sulfonate anion from the PBDT double helix and low molecular weight PEG. We discuss our mechanical and conductivity results based on this proposed model.

Based on the imaged morphology, we propose a model for the self-assembled structure of PBDT rigid-rods and PEG in these membranes, as depicted in **Figure 1d** and **Figure 1e**. At the scale of ~ 100 nm (**Figure 1d**), the membranes have a biphasic environment of PBDT-rich and PBDT-poor regions, similar to previous studies in MICs.<sup>25</sup> At the scale of ~ 2 nm within a PBDT bundle (**Figure 1e**), the counterions are able to interact with both the sulfonate groups from the PBDT double helix and with PEG. By tuning both the counterion and PBDT weight fraction, these ionic interactions at both of these length scales are able to affect both the mechanical and conductive properties of these solid membranes, which will be discussed further below.

To quantitatively describe these two phases, we calculated the volume fraction of PBDT-rich bundles and PEG-rich puddles through a similar method as previously applied to the MICs with varying ionic liquids (ILs). <sup>28</sup> Using this method, we determined that the average PBDT bundle diameter is approximately  $14 \pm 3$  nm with a rod-rod spacing of 2.2 nm in a hexagonal lattice (based on volumetric estimates of initial and final material compositions and densities, <sup>24</sup> and MD calculations from Yu et al. <sup>31</sup>), and each bundle has approximately  $40 \pm 10$  PBDT double helical rods. Additionally, we determined the volume fraction of PBDT rods in the PBDT-PEG membrane ( $\phi_{\text{total}}$ ), the volume fraction of PBDT rods in a PBDT bundle ( $\phi_{\text{bundle}}$ ), the volume fraction of bundle in the membrane ( $\phi_{\text{total}}$ ), and the volume fraction of PEG-rich regions in the membrane ( $1 - \frac{1}{2}$ ).

 $\varphi_{\text{total}}/\varphi_{\text{bundle}}$ ) (values listed in **Table S3**). Based on our calculations, increasing either the NaPBDT or LiPBDT concentration in the membranes leads to an increase of the PBDT bundle phase volume fraction, diminishing the contribution of the liquid-like behavior of the PEG-rich phase. Note that the bundle volume fraction calculations for some of the membranes achieve values greater than 1 at elevated PBDT concentration. Since theoretically there are no PEG puddles in these membranes, this may suggest that more PBDT rods are introduced into each bundle, increasing  $\varphi_{\text{bundle}}$ .

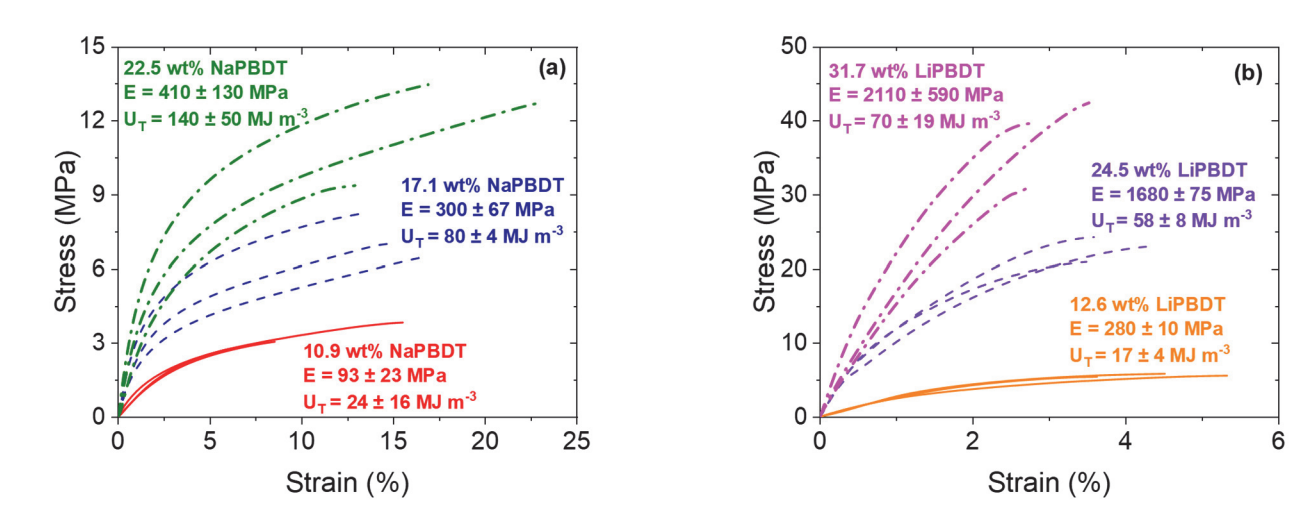


Figure 2: Mechanical robustness of the PBDT-PEG membranes. Uniaxial stress-strain curves for the PBDT-PEG membranes with (a) Na<sup>+</sup> counterions and (b) Li<sup>+</sup> counterions at a force ramp rate of 1 N min<sup>-1</sup> at 30 °C. All membranes were repeated by cutting three test samples from each PBDT-PEG membrane. The slope of the stress-strain curves at < 0.5% strain yields the Young's modulus (E), with values of E and the toughness ( $U_T$ ) with standard deviations.

In addition to varying the morphology, the variation in the PBDT-rich and PBDT-poor volume fractions at different PBDT concentrations leads to varying mechanical properties in the PBDT-PEG membranes, which are crucial for practical applications. **Figure 2** shows the uniaxial stress-strain curves for the NaPBDT-PEG and LiPBDT-PEG membranes respectively at 30  $^{\circ}$ C with the resulting Young's modulus (*E*) and the toughness (*U*<sub>T</sub>) listed for each membrane (a full list of mechanical properties, including the tensile strength and strain at break is listed in **Table S4**).

From these measurements, the PBDT-PEG membranes show three distinct trends: (1) increasing the PBDT concentration leads to an enhancement in E, tensile strength, and toughness, (2) incorporating a smaller alkali counterion (Li<sup>+</sup>) leads to enhanced mechanical properties in the membranes, with the 31.7 wt% LiPBDT membrane producing a E of roughly 2.1 GPa and a tensile strength of 38 MPa, and (3) incorporating a larger alkali counterion (Na<sup>+</sup>) leads to enhanced ductile behavior and toughness, with the 22.5 wt% NaPBDT membrane reaching a maximum toughness of  $\sim 140$  MJ m<sup>-3</sup>. These results are consistent with previous tensile tests done on MIC membranes with varying PBDT concentration as well as cations that associate variably with the PBDT sulfonate groups, where increasing the PBDT concentration enhances the stiffness and the tensile strength in the MIC.<sup>23, 24</sup> In terms of the different mechanical responses between the NaPBDT-PEG and LiPBDT-PEG membranes, we propose that the PEG-solvated Li<sup>+</sup> counterions have stronger ionic interactions with the PBDT sulfonate groups than the Na<sup>+</sup> counterions, leading to more PEG incorporated into the PBDT bundle phase. It is also very interesting that the mechanical properties, especially the Young's modulus of the LiPBDT-PEG samples, are quite comparable with the NaPBDT-Pyr<sub>14</sub>TFSI MICs at similar polymer content.<sup>29</sup> This further indicated that the collective electrostatic network in MICs contributes to their mechanical rigidity.

### **Charge Transport and Dielectric Relaxation**

We investigate the effect of NaPBDT or LiPBDT concentration on the charge transport of the PBDT-PEG membranes through their ionic conductivity ( $\sigma_0$ ) using dielectric relaxation spectroscopy. **Figure 3a** shows the temperature dependence of the  $\sigma_0$  for the PBDT-PEG membranes taken in the regime where the imaginary part of permittivity ( $\varepsilon''$ ) ~  $\omega^{-1}$  and  $\sigma_0 = \omega \varepsilon_0 \varepsilon''$ .<sup>33, 34</sup> At 30 °C, the conductivity of these electrolytes ranges from 0.14  $\mu$ S cm<sup>-1</sup> to 7.2  $\mu$ S cm<sup>-1</sup>, and the conductivity decreases with PBDT concentration indicating that the average mobility of

Li<sup>+</sup>/Na<sup>+</sup> is the limiting factor (**Figure S3**). The electrolytes with Na<sup>+</sup> as the counterion demonstrate significantly higher conductivity, presumably due to the weaker interactions between sulfonate groups and Na<sup>+</sup> compared to Li<sup>+</sup>. The temperature dependence of  $\sigma_0$  is fitted using the Vogel-Fulcher-Tammann (VFT) equation,

$$\sigma_o(T) = \sigma_\infty \exp\left(-\frac{BT_0}{T - T_0}\right) \tag{1}$$

where  $\sigma_{\infty}$  is the infinite temperature conductivity limit, B is a strength parameter reciprocally related to the fragility, and  $T_0$  is the Vogel temperature (VFT parameters listed in **Table S5**).

The ionic conductivity of the NaPBDT membranes is consistently higher than the LiPBDT membranes, with the 10.9 wt% NaPBDT membrane reaching a room temperature  $\sigma_0$  of 7.2  $\mu$ S cm<sup>-1</sup> and a maximum conductivity of 0.13 mS cm<sup>-1</sup> at 120 °C. The highest  $\sigma_0$  in the LiPBDT membranes is from the 12.6 wt% membrane (2  $\mu$ S cm<sup>-1</sup> at room temperature and 40  $\mu$ S cm<sup>-1</sup> at 120 °C). This is most likely due to the Li<sup>+</sup> ion being a stronger Lewis acid than Na<sup>+</sup>, thus requiring a larger amount of energy for the Li<sup>+</sup> ions to dissociate from the PEG in between the PBDT rods.<sup>35</sup> We suspect that the stronger Lewis acidity also accounts for the two LiPBDT membranes with higher PBDT concentrations to have low fragility, making them stronger glass formers.

In addition to the counterion differences, we also show that increasing the PEG content in the membranes enhances the ionic conductivity, consistent with previous studies where increasing the ratio of PEG-based group to the ionic-based group increased  $\sigma_0$ .<sup>36</sup> This is due to the PEG providing a polar medium for counterions to undergo charge transport, since PEG has a measured dielectric constant of ~ 17 at room temperature.<sup>37</sup> The idea of the polar medium is shown further in **Table 1** through the static dielectric constant ( $\varepsilon_s$ ) and the Coulombic dielectric constant ( $\varepsilon_c$ ). By incorporating more NaPBDT or LiPBDT into the membrane, the dielectric constant attributed to

the PEG dipole,  $\varepsilon_C$ , decreases which increases the amount of energy required for the dissociation of ion pairs from aggregates in the PBDT-rich phase. This reduces the polarizability of these membranes and lowers their ionic conductivity (the determination of the dielectric constants in the PBDT-PEG membranes is described in SI and is shown through **Figure S4**). Wang et al. showed that incorporating Li<sup>+</sup> or Na<sup>+</sup> counterions with a poly(ethylene oxide) based polymer and a tethered sulfonate group produced ion aggregates at elevated temperatures.<sup>38</sup> However, while Na<sup>+</sup> counterions were able to dissociate into ion pairs as the temperature decreased, the Li<sup>+</sup> counterions form ionic aggregates at lower temperatures, leading to a lower  $\varepsilon_8$  than the polymers with larger counterions.

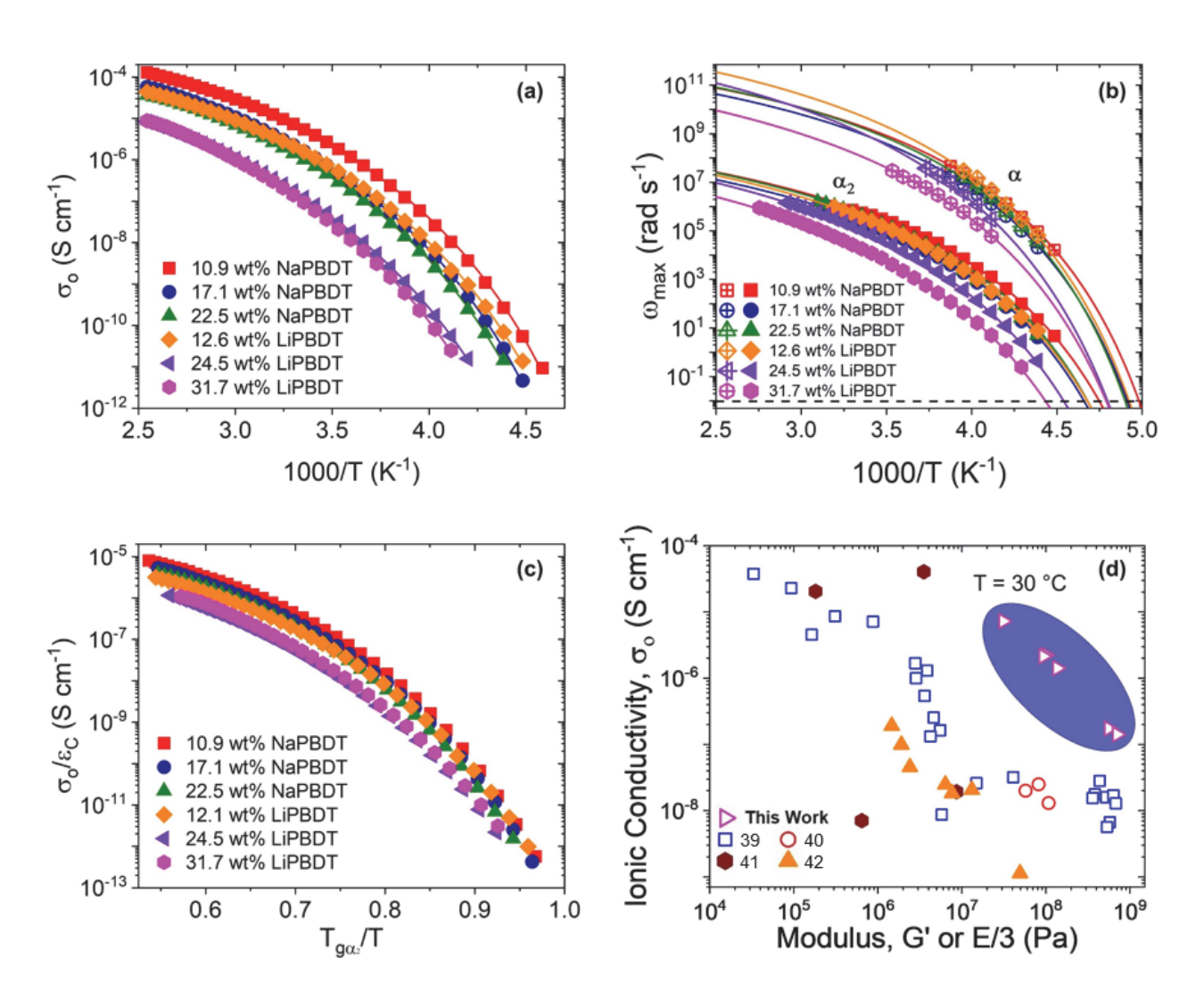


Figure 3: Charge transport, dielectric relaxation, and relationship between the ionic conductivity and the modulus of PBDT-PEG membranes. (a) Temperature dependence of the ionic conductivity ( $\sigma_0$ ) for the PBDT-PEG membranes with varying PBDT concentration and varying conductive counterion. All  $\sigma_0$  are fit to the VFT equation (Eq. (1), solid lines) with their parameters listed in **Table S4**. (b) Temperature-dependent peak relaxation frequencies ( $\omega_{max}$  and  $\omega_{max_2}$ ) of the single-ion PBDT-PEG membranes. Data are fit to the VFT equation with parameters listed in Table S5 and with the same Vogel temperature as the ionic conductivity. Fits were extrapolated down to 10<sup>-2</sup> rad s<sup>-1</sup> (100 s, dashed line) to give the dynamic glass transition temperature  $(T_g)$  in DRS from the  $\alpha_2$  relaxation shown in **Table 1** with comparisons to the DSC  $T_{\rm g}$ . (c) Temperature dependence normalized by the DRS glass transition temperature of the ionic conductivity divided by the Coulombic dielectric constant ( $\sigma_0/\varepsilon_C$ ) for the PBDT-PEG membranes. (d) Relationship between the ionic conductivity ( $\sigma_0$ ) and the modulus (either G' or E/3) for PBDT-PEG membranes and various polymer single-ion conducting electrolytes<sup>39-42</sup> at 30 °C. Reference numbers are given in the figure legend where filled symbols represent materials with recorded shear moduli (G') and open symbols represent materials with recorded tensile moduli (E). The PBDT-PEG membranes consistently show either higher moduli or  $\sigma_0$  when compared to other single-ion polymer electrolytes. The experimental errors are smaller than the symbol sizes.

**Table 1:** Measured values for the ionic conductivity ( $\sigma_0$ ) at 30 °C, static dielectric constant ( $\varepsilon_s$ ) and Coulombic dielectric constant ( $\varepsilon_c$ ) at -20 °C, DSC  $T_g$  and DRS  $T_g$  from the  $\alpha$  and  $\alpha_2$  relaxation processes in the PBDT-PEG membranes.

Sample	$\sigma_{\rm o}$ at 30 °C	$\varepsilon_{\rm s}$ at $-20~^{\circ}{ m C}$	$\varepsilon_{\rm C}$ at $-20^{\circ}{\rm C}$	$DSC T_g$	DRS $T_{g\alpha}$	DRS $T_{g\alpha 2}$
	(µS cm <sup>-1</sup> )			(K)	(K)	(K)
10.9 wt% NaPBDT	7.2	36	16	205	201	211
17.1 wt% NaPBDT	2.2	31	11	210	204	215
22.5 wt% NaPBDT	1.4	27	9.3	210	204	215
12.6 wt% LiPBDT	2.1	28	14	202	203	214
24.5 wt% LiPBDT	0.2	19	7.2	214	208	220
31.7 wt% LiPBDT	0.1	48	8.1	226	209	226

To further explore the charge transport in the PBDT-PEG membranes, we analyze the dielectric relaxations that occur in these membranes over a wide temperature range. **Figure 3b** shows the temperature dependence of the peak relaxation frequencies of the two relaxation processes ( $\alpha$  and  $\alpha$ <sub>2</sub>) observed in these membranes, and they are fit to the VFT equation,

$$\omega_{max} = \omega_{\infty} \exp\left(-\frac{BT_0}{T - T_0}\right) \tag{2}$$

where  $\omega_{\infty}$  is the relaxation frequency at infinite temperature, B is a dimensionless parameter reciprocally related to fragility and T<sub>0</sub> is the Vogel temperature determined from the VFT fit to the ionic conductivity (Eq. (1)). Further analysis on how  $\omega_{\text{max}}$  is determined in the PBDT-PEG membranes is described in SI and is shown in Figure S5 with VFT parameters listed in Table S6. Increasing the PBDT concentration leads to a retardation of both  $\alpha$  and  $\alpha_2$  relaxations, which are attributed to the segmental motion of the PEG and the counterion dissociation prior to electrode polarization respectively. We propose that the latter relaxation process is due to the counterion motion since this process is broadly coupled with the timescale of the diffusive conductive motion of the counterions (Figure S6). From these relaxation processes, we explore the effects of the glassy dynamics on the charge transport by dividing the ionic conductivities of the PBDT-PEG membranes by their respective  $\varepsilon_{\rm C}$ . Figure 3c shows the normalized conductivity as a function of temperature normalized by Tg determined in DRS and highlights that all reduced ionic conductivities of the membranes roughly collapse onto a single curve at lower temperatures (SI Note 9 further describes determination of the DRS  $T_g$  values.). The higher LiPBDT concentration membranes are stronger glass-formers with stronger ionic interactions. However, due to the near agreement in the reduced conductivities, we conclude that the counterion transport in these membranes depends mostly on two factors: (1) the dynamics of the diffusive motion of the counterions, dictated by the glass transition, and (2) the dissociation of ion-pairs allowing for more counterions to contribute to the conductivity, dictated by the coulombic dielectric constant.<sup>43</sup>

#### Conclusion

We assembled single-ion conducting solid polymer electrolytes using low molecular weight PEG and the rigid-rod PBDT polyelectrolyte with either Na<sup>+</sup> or Li<sup>+</sup> counterions. These materials exhibit biphasic internal structures wherein the volume fraction of the PEG-rich phase

decreases as the PBDT concentration increases in the membrane. Incorporating mobile Na<sup>+</sup> yields membranes with higher ductility and faster charge transport, while membranes with Li<sup>+</sup> have higher mechanical strength and slower charge transport. We suspect this arises from weaker Li<sup>+</sup> dissociation from the sulfonate groups, and stronger ionic/dipolar interactions between the LiPBDT and PEG. These observations confirm that the modulus of PBDT-based materials strongly depends on the ionic interactions that exists in the PBDT-bundle phase. Comparing these PBDT-PEG membranes with other solid-state polymer electrolytes (**Figure 3d**) shows that while these PBDT-PEG membranes do not produce high ionic conductivities compared to salt-loaded systems, they do exhibit substantially higher ionic conductivity and modulus when compared to other single-ion-conducting electrolytes.<sup>39-42</sup> Overall, this study shows that mechanically strong solid polymer electrolytes with high ionic conductivity can be obtained from a low molecular weight PEG and a rigid-rod polyanion.

#### **Experimental Section**

*Materials:* Both the LiPBDT and NaPBDT were synthesized as previously reported.<sup>26, 44</sup> Aqueous solutions of PBDT were prepared by combining NaPBDT or LiPBDT and deionized water in vials. The LiPBDT aqueous solution and NaPBDT aqueous solution show transitions to the fully nematic phase at 1.9 wt% PBDT, and thus their properties only differ according to their counterions (Li<sup>+</sup> or Na<sup>+</sup>). Poly(ethylene glycol) with average molecular weight of 400 g mol<sup>-1</sup> (PEG400), was purchased from Sigma-Aldrich. N, N-dimethylformamide (DMF) was purchased from Fisher Scientific.

*Membrane Preparation:* The PBDT-PEG membranes were prepared similarly to related materials previously reported.<sup>26, 29</sup> As an example, to prepare the 24.5 wt% LiPBDT-PEG membrane, 0.15

g of LiPBDT was dissolved in 15 g of H<sub>2</sub>O while 0.86 g of PEG was dissolved in 7.5 g of DMF. After heating both solutions to 85 °C, both solutions are mixed together and equilibrated in a tightly capped vial inside a Yamato DX600 oven at 85 °C overnight. The mixed solution was then poured onto a glass dish and dried at 85 °C for 24 h. The transparent and free-standing membrane was then peeled off and further dried under vacuum at 60 °C for 2 days. The final mass of the membrane was 0.62 g, giving a calculated PBDT concentration in the dried membrane at roughly 24.5 wt% after vacuum drying. The remaining membranes were prepared the same way with **Table S1** listing the weights of the materials used to prepare each casting solution as well as the mass of each sample after vacuum drying. We found that the masses of the final dried membranes are less than the corresponding overall masses of PBDT and PEG used to prepare the casting solutions. We attribute the mass loss to evaporation of PEG. When using PEG with ether end groups, the mass loss is more significant. Thus, we used hydroxyl terminated PEG in this study, even though etherterminated PEG should be incorporated (using a more optimized film casting process) to achieve practical use as hydroxyl groups are reactive at interfaces in typical non-aqueous rechargeable batteries. The current casting method yielded three Na<sup>+</sup> conducting electrolytes with 10.9, 17.1, and 22.5 wt% NaPBDT and three Li<sup>+</sup> conducting electrolytes containing 12.6, 24.5, and 31.7 wt% LiPBDT.

Atomic Force Microscopy (AFM): AFM images of the PBDT-PEG membranes were collected in tapping mode using a Veeco Bioscope II system at room temperature. Each sample was scanned over a 1 μm<sup>2</sup> surface.

Mechanical Properties: Tensile stress-strain measurements were carried out using a TA Q800 dynamic mechanical analyzer. Prior to all measurements, the PBDT-PEG membranes were cut into strips and dried under vacuum for 24 h at 80 °C. Once loaded into the sample clamps, all

membranes were equilibrated at 30 °C for 5 min. Once equilibrated, stress-strain measurements were carried out at a force ramp rate of 1 N min<sup>-1</sup> until the sample broke. Each measurement was then repeated two more times with different cuts from the same membrane, resulting in three stress-strain curves for each membrane.

Thermal Analysis: Prior to any temperature-dependent measurements, thermogravimetric analysis (TGA) was conducted to verify the thermal stability of the PBDT-PEG membranes under nitrogen at a 10 °C min<sup>-1</sup> heating rate over a temperature range from 25 - 700 °C using a TA Instruments Q600 (shown in Supporting Information **Figure S1**). Glass transition temperatures ( $T_g$ ) of the PBDT-PEG membranes and pure PEG400 were measured through differential scanning calorimetry (DSC) using a TA Instruments DSC Q2000 (**Figure S2**).  $T_g$  was determined as the change in heat capacity in the second heating scan at 5 °C min<sup>-1</sup> (DSC  $T_g$  and thermal stability of PBDT-PEG membranes at 95% original mass ( $T_{d.95\%}$ ) are listed in **Table S2**).

Dielectric Relaxation Spectroscopy (DRS): Dielectric measurements of the PBDT-PEG membranes were carried out through DRS using a Novocontrol GmbH Concept 40 broadband dielectric spectrometer. The thickness of the sample was measured using a micrometer. Each membrane with varying composition of PBDT and PEG400 was pressed in between a polished 10 mm brass electrode and a polished 30 mm brass electrode and placed under vacuum at 80 °C for 1 h for the membranes to adhere to the electrodes. Once annealed under vacuum, the membranes were loaded into the Novocontrol and annealed at 120 °C under nitrogen for an hour to remove any moisture picked up during sample loading. Isothermal dielectric data were then collected using a sinusoidal voltage with an amplitude of 0.1 V over a frequency range of 10<sup>-1</sup> – 10<sup>7</sup> Hz. Measurements were carried out in steps of 5 °C in cooling from 120 °C to -100 °C followed by steps of 10 °C in heating from -100 °C to 120 °C.

**Associated Content** 

**Supplementary Information** 

Masses of PBDT and solvents used to prepare the PBDT-PEG membranes, thermal stability of the

PBDT-PEG membranes, DSC analysis of neat PEG400 and PBDT-PEG membranes, VFT fitting

parameters for the ionic conductivity and ion concentration dependence on the conductivity,

determination of the static and coulombic dielectric constants, dielectric relaxations and glass

transitions in PBDT-PEG membranes, ratio of the conductive and ion rearrangement timescales.

**Author Information** 

**Corresponding Authors** 

\*Email: rhc@plmsc.psu.edu (R.H.C)

\*Email: lmadsen@vt.edu (L.A.M)

**ORCID** 

Joshua E. Bostwick: 0000-0002-0640-5223

Deyang Yu: 0000-0003-0587-1211

Curt J. Zanelotti: 0000-0003-2622-7345

Theo J. Dingemans: 0000-0002-8559-2783

Louis A. Madsen: 0000-0003-4588-5183

Ralph H. Colby: 0000-0002-5492-6189

**Notes** 

The authors declare no competing financial interest.

17

# Acknowledgments

The authors would like to thank Dr. Stephen McCartney for conducting the AFM measurements. We are also very grateful for the support from the National Science Foundation under the DMR 1807934 and 1810194 awards, and the support by the U.S. Department of Energy's Office of Energy Efficiency and Renewable Energy (EERE) under Award No. DE-EE0008860.

#### References

- 1. Liang, Y.; Zhao, C.-Z.; Yuan, H.; Chen, Y.; Zhang, W.; Huang, J.-Q.; Yu, D.; Liu, Y.; Titirici, M.-M.; Chueh, Y.-L.; Yu, H.; Zhang, Q., A review of rechargeable batteries for portable electronic devices. *InfoMat* **2019**, *I* (1), 6-32.
- 2. Manthiram, A., An Outlook on Lithium Ion Battery Technology. *ACS Central Science* **2017**, *3* (10), 1063-1069.
- 3. Liu, Z.; Li, H.; Zhu, M.; Huang, Y.; Tang, Z.; Pei, Z.; Wang, Z.; Shi, Z.; Liu, J.; Huang, Y.; Zhi, C., Towards wearable electronic devices: A quasi-solid-state aqueous lithiumion battery with outstanding stability, flexibility, safety and breathability. *Nano Energy* **2018**, *44*, 164-173.
- 4. Duan, J.; Tang, X.; Dai, H.; Yang, Y.; Wu, W.; Wei, X.; Huang, Y., Building Safe Lithium-Ion Batteries for Electric Vehicles: A Review. *Electrochemical Energy Reviews* **2020**, *3* (1), 1-42.
- 5. Li, Q.; Chen, J.; Fan, L.; Kong, X.; Lu, Y., Progress in electrolytes for rechargeable Libased batteries and beyond. *Green Energy & Environment* **2016**, *1* (1), 18-42.
- 6. Bocharova, V.; Sokolov, A. P., Perspectives for Polymer Electrolytes: A View from Fundamentals of Ionic Conductivity. *Macromolecules* **2020**, *53* (11), 4141-4157.
- 7. Tarascon, J. M.; Armand, M., Issues and challenges facing rechargeable lithium batteries. *Nature* **2001**, *414* (6861), 359-367.
- 8. Fenton, D. E.; Parker, J. M.; Wright, P. V., Complexes of alkali metal ions with poly(ethylene oxide). *Polymer* **1973**, *14* (11), 589.
- 9. Long, L.; Wang, S.; Xiao, M.; Meng, Y., Polymer electrolytes for lithium polymer batteries. *J. Mater. Chem. A* **2016**, *4* (26), 10038-10069.
- 10. Mindemark, J.; Lacey, M. J.; Bowden, T.; Brandell, D., Beyond PEO—Alternative host materials for Li+-conducting solid polymer electrolytes. *Prog. Polym. Sci.* **2018**, *81*, 114-143.
- 11. Tikekar, M. D.; Choudhury, S.; Tu, Z.; Archer, L. A., Design principles for electrolytes and interfaces for stable lithium-metal batteries. *Nat. Energy* **2016**, *I* (9), 16114.
- 12. Zhu, J.; Zhang, Z.; Zhao, S.; Westover, A. S.; Belharouak, I.; Cao, P.-F., Single-Ion Conducting Polymer Electrolytes for Solid-State Lithium–Metal Batteries: Design, Performance, and Challenges. *Adv. Energy Mater.* **2021**, *11* (14), 2003836.

- 13. Rosso, M.; Gobron, T.; Brissot, C.; Chazalviel, J. N.; Lascaud, S., Onset of dendritic growth in lithium/polymer cells. *Journal of Power Sources* **2001**, *97-98*, 804-806.
- 14. Song, J. Y.; Wang, Y. Y.; Wan, C. C., Review of gel-type polymer electrolytes for lithium-ion batteries. *Journal of Power Sources* **1999**, *77* (2), 183-197.
- 15. Zhu, M.; Wu, J.; Wang, Y.; Song, M.; Long, L.; Siyal, S. H.; Yang, X.; Sui, G., Recent advances in gel polymer electrolyte for high-performance lithium batteries. *Journal of Energy Chemistry* **2019**, *37*, 126-142.
- 16. Kuray, P.; Mei, W.; Sheffield, S. E.; Sengeh, J.; Pulido, C. R. F.; Capparelli, C.; Hickey, R. J.; Hickner, M. A., Ion Transport in Solvated Sodium-Ion Conducting Gel Polymer Electrolytes. *Frontiers in Energy Research* **2020**, *8* (250).
- 17. Xi, J.; Qiu, X.; Ma, X.; Cui, M.; Yang, J.; Tang, X.; Zhu, W.; Chen, L., Composite polymer electrolyte doped with mesoporous silica SBA-15 for lithium polymer battery. *Solid State Ionics* **2005**, *176* (13), 1249-1260.
- 18. Kuo, P.-L.; Wu, C.-A.; Lu, C.-Y.; Tsao, C.-H.; Hsu, C.-H.; Hou, S.-S., High Performance of Transferring Lithium Ion for Polyacrylonitrile-Interpenetrating Crosslinked Polyoxyethylene Network as Gel Polymer Electrolyte. *ACS Applied Materials & Interfaces* **2014**, *6* (5), 3156-3162.
- 19. Ito, A.; Yasuda, T.; Yoshioka, T.; Yoshida, A.; Li, X.; Hashimoto, K.; Nagai, K.; Shibayama, M.; Watanabe, M., Sulfonated Polyimide/Ionic Liquid Composite Membranes for CO2 Separation: Transport Properties in Relation to Their Nanostructures. *Macromolecules* **2018**, *51* (18), 7112-7120.
- 20. Mantravadi, R.; Chinnam, P. R.; Dikin, D. A.; Wunder, S. L., High Conductivity, High Strength Solid Electrolytes Formed by in Situ Encapsulation of Ionic Liquids in Nanofibrillar Methyl Cellulose Networks. *ACS Applied Materials & Interfaces* **2016**, *8* (21), 13426-13436.
- 21. Wang, Y.; He, Y.; Yu, Z.; Gao, J.; ten Brinck, S.; Slebodnick, C.; Fahs, G. B.; Zanelotti, C. J.; Hegde, M.; Moore, R. B.; Ensing, B.; Dingemans, T. J.; Qiao, R.; Madsen, L. A., Double helical conformation and extreme rigidity in a rodlike polyelectrolyte. *Nature Communications* **2019**, *10* (1), 801.
- 22. Wu, Z. L.; Arifuzzaman, M.; Kurokawa, T.; Le, K.; Hu, J.; Sun, T. L.; Furukawa, H.; Masunaga, H.; Gong, J. P., Supramolecular Assemblies of a Semirigid Polyanion in Aqueous Solutions. *Macromolecules* **2013**, *46* (9), 3581-3586.

- 23. Fox, R. J.; Yu, D.; Hegde, M.; Kumbhar, A. S.; Madsen, L. A.; Dingemans, T. J., Nanofibrillar Ionic Polymer Composites Enable High-Modulus Ion-Conducting Membranes. *ACS Applied Materials & Interfaces* **2019**, *11* (43), 40551-40563.
- 24. Wang, Y.; Chen, Y.; Gao, J.; Yoon, H. G.; Jin, L.; Forsyth, M.; Dingemans, T. J.; Madsen, L. A., Highly Conductive and Thermally Stable Ion Gels with Tunable Anisotropy and Modulus. *Advanced Materials* **2016**, *28* (13), 2571-2578.
- 25. Bostwick, J. E.; Zanelotti, C. J.; Iacob, C.; Korovich, A. G.; Madsen, L. A.; Colby, R. H., Ion Transport and Mechanical Properties of Non-Crystallizable Molecular Ionic Composite Electrolytes. *Macromolecules* **2020**, *53* (4), 1405-1414.
- 26. Yu, D.; Pan, X.; Bostwick, J. E.; Zanelotti, C. J.; Mu, L.; Colby, R. H.; Lin, F.; Madsen, L. A., Room Temperature to 150 °C Lithium Metal Batteries Enabled by a Rigid Molecular Ionic Composite Electrolyte. *Advanced Energy Materials* **2021**, *11* (12), 2003559.
- 27. Wang, Y.; Zanelotti, C. J.; Wang, X.; Kerr, R.; Jin, L.; Kan, W. H.; Dingemans, T. J.; Forsyth, M.; Madsen, L. A., Solid-state rigid-rod polymer composite electrolytes with nanocrystalline lithium ion pathways. *Nature Materials* **2021**, *20* (9), 1255-1263.
- 28. Bostwick, J. E.; Zanelotti, C. J.; Yu, D.; Pietra, N. F.; Williams, T. A.; Madsen, L. A.; Colby, R. H., Ionic interactions control the modulus and mechanical properties of molecular ionic composite electrolytes. *Journal of Materials Chemistry C* **2022**, *10* (3), 947-957.
- 29. Yu, D.; Zanelotti, C. J.; Fox, R. J.; Dingemans, T. J.; Madsen, L. A., Solvent-Cast Solid Electrolyte Membranes Based on a Charged Rigid-Rod Polymer and Ionic Liquids. *ACS Applied Energy Materials* **2021**, *4* (7), 6599-6605.
- 30. Bostwick, J. E. Investigation of Charge Transport and Mechanical Properties in Ion Associating Polymeric Materials. The Pennsylvania State University, 2021.
- 31. Yu, Z.; He, Y.; Wang, Y.; Madsen, L. A.; Qiao, R., Molecular Structure and Dynamics of Ionic Liquids in a Rigid-Rod Polyanion-Based Ion Gel. *Langmuir* **2017**, *33* (1), 322-331.
- 32. Yu, D. Preparation, Characterization, and Application of Molecular Ionic Composities for High Performance Batteries. Virginia Polytechnic Institute and State University, 2021.
- 33. Kremer, F.; Schönhals, A., *Broadband Dielectric Spectroscopy*. Springer, Berlin, Heidelberg: New York, 2003.
- 34. Leys, J.; Wübbenhorst, M.; Menon, C. P.; Rajesh, R.; Thoen, J.; Glorieux, C.; Nockemann, P.; Thijs, B.; Binnemans, K.; Longuemart, S., Temperature dependence of the

- electrical conductivity of imidazolium ionic liquids. *The Journal of Chemical Physics* **2008**, *128* (6), 064509.
- 35. Sagane, F.; Abe, T.; Iriyama, Y.; Ogumi, Z., Li+ and Na+ transfer through interfaces between inorganic solid electrolytes and polymer or liquid electrolytes. *Journal of Power Sources* **2005**, *146* (1), 749-752.
- 36. Wang, J.-H. H.; Yang, C. H.-C.; Masser, H.; Shiau, H.-S.; O'Reilly, M. V.; Winey, K. I.; Runt, J.; Painter, P. C.; Colby, R. H., Ion States and Transport in Styrenesulfonate Methacrylic PEO9 Random Copolymer Ionomers. *Macromolecules* **2015**, *48* (19), 7273-7285.
- 37. Sengwa, R. J.; Kaur, K.; Chaudhary, R., Dielectric properties of low molecular weight poly(ethylene glycol)s. *Polymer International* **2000**, *49* (6), 599-608.
- 38. Wang, W.; Tudryn, G. J.; Colby, R. H.; Winey, K. I., Thermally Driven Ionic Aggregation in Poly(ethylene oxide)-Based Sulfonate Ionomers. *Journal of the American Chemical Society* **2011**, *133* (28), 10826-10831.
- 39. Snyder, J. F.; Carter, R. H.; Wetzel, E. D., Electrochemical and Mechanical Behavior in Mechanically Robust Solid Polymer Electrolytes for Use in Multifunctional Structural Batteries. *Chemistry of Materials* **2007**, *19* (15), 3793-3801.
- 40. Xu, H.-S.; Yang, C.-Z., The ionic conductive property of sulfonated polyethylene oxide polyurethane ionomers. *Journal of Polymer Science Part B: Polymer Physics* **1995**, *33* (5), 745-751.
- 41. Wang, S.-W.; Colby, R. H., Linear Viscoelasticity and Cation Conduction in Polyurethane Sulfonate Ionomers with Ions in the Soft Segment–Multiphase Systems. *Macromolecules* **2018**, *51* (8), 2767-2775.
- 42. Wang, J.-H. Conductivity, Morphology, and Dynamics of Single-Ion Conducting Random and Block Copolymers. Pennsylvania State University, 2015.
- 43. Choi, U. H.; Price, T. L.; Schoonover, D. V.; Xie, R.; Gibson, H. W.; Colby, R. H., Role of Chain Polarity on Ion and Polymer Dynamics: Molecular Volume-Based Analysis of the Dielectric Constant for Polymerized Norbornene-Based Ionic Liquids. *Macromolecules* **2020**, *53* (23), 10561-10573.
- 44. Gao, J.; Wang, Y.; Norder, B.; Garcia, S. J.; Picken, S. J.; Madsen, L. A.; Dingemans, T. J., Water and sodium transport and liquid crystalline alignment in a sulfonated aramid membrane. *Journal of Membrane Science* **2015**, *489*, 194-203.